Synthesis of $NiCo_2S_4$@$NiMoO_4$ Nanosheets with Excellent Electrochemical Performance for Supercapacitor

Yucai Li (hjhj6758_sk@126.com)
Shenyang Institute of Engineering
Yan Zhao
Shenyang Institute of Engineering
Shiwei Song
Shenyang Institute of Engineering
Jian wang
Shenyang Institute of Engineering

Research Article

Keywords: NiCo2S4@NiMoO4, Electrochemical performance, Battery-type electrode, Asymmetric supercapacitor, Cyclic stability

Posted Date: June 22nd, 2021

DOI: https://doi.org/10.21203/rs.3.rs-641149/v1

Abstract

Core-shell structured $NiCo_2S_4$@$NiMoO_4$ is considered to be one of the most promising electrode materials for supercapacitors due to its high specific capacitance and excellent cycle performance. In this work, we report $NiCo_2S_4$@$NiMoO_4$ nanosheets on Ni foam by two-step fabricated method. The as-obtained product has high capacitance of 1102.5 F g^{-1} at 1 A g^{-1}. The as-assembled supercapacitor has also a high energy density of 37.6 W h kg^{-1} and superior cycle performance with 85% capacitance retention. The electrode materials reported here might exhibits potential applications in future energy storage devices.

Introduction

Rapid development of economy and society leads to the growing demand for energy. Due to the serious shortage of traditional fossil fuels and the deterioration of the environment, it is urgent to design and develop sustainable devices for energy storage and conversion [1–3]. Among all kinds of energy storage equipment, supercapacitor is widely concerned for its fast charge-discharge rate, high power density, long cycling life and environment-benign behavior [4–6]. However, the low energy density of supercapacitor limits their further application in the field of energy storage. According to the different charge storage mechanism, supercapacitor electrodes can be classified into electric double layer electrodes and pseudo-capacitors [7,8]. The energy storage of pseudocapacitive electrode materials mainly depends on Faraday redox reaction, which makes the specific capacitance and energy density of pseudocapacitive electrode higher than that of EDLEs [9–11]. The materials of pseudo-capacitors mainly include transition metal oxides, nitrides, sulfides and conducting polymers.

Transition metal sulfide have been proved to be reliable electrode materials for supercapacitor, which have better electron conductivity and cycling stability than metal oxides [12, 13]. Among them, $NiCo_2S_4$ is considered to be one of the most promising electrode materials for supercapacitors because of its unique atomic structure and electronic properties [14, 15]. Especially, $NiMoO_4$ is provided with high theoretical capacity, excellent rate performance, good conductivity and high redox reversibility. However, cycle performance and specific capacitance usually restricts their electrochemical performance. In order to deal with above issues, Various nanostructures of $NiCo_2S_4$/$NiMoO_4$ nanostructures, such as nanorods, nanosheet arrays, nanoneedle-sheets and core-shell structures have been explored as electrode materials for supercapacitors, and have been proved to have excellent electrochemical properties [16–18]. However, the single electrode materials are limited by their slow reaction kinetics, moderate active sites, unstable structure, poor cycle stability and low rate performance [19]. Therefore, it is still a great challenge to design and prepare structurally stable $NiCo_2S_4$@$NiMoO_4$ electrode materials.

Herein, we synthesized $NiCo_2S_4$@$NiMoO_4$ on Ni foam using a two-step method. The nanosheets structure provides a shorter transport path for ions and electrons. The $NiCo_2S_4$@$NiMoO_4$nanosheets as supercapacitor electrode materials shows high capacitance of 1102.5 F g^{-1} at a current density of 1 A g^{-1} and capacitive retention of 72.7 % after 10000 cycles. Moreover, an asymmetric supercapacitor is

constructed by $NiCo_2S_4$@$NiMoO_4$ structures as positive electrode and active carbon as negative electrode. It possesses an energy density of 36.5 W h kg^{-1} at power density of 2880 W kg^{-1}. These excellent electrochemical performances could be credited to its unique nanosheets structure.

Experimental

2.1 Synthesis of $NiCo_2S_4$@$NiMoO_4$ structure

At first, $NiCo_2S_4$ nanosheets were grown on Ni foam by a simple solvothermal method. 1 mM $NiCl_2$•$6H_2O$, 2 mM $CoCl_2$•$6H_2O$, 1.0 g Urea and 0.6 g NH_4F were dissolved in 40 ml solution of deionized water and stirred for 30 min under constant magnetic force. Then, the above solution with the pretreated Ni foam was transferred into an 80 mL autoclave and kept at 100°C for 8 h. After natural cooling down to room temperature naturally, the as-synthesized samples were got out and washed with deionized water. $NiCo_2S_4$ was prepared through a vulcanization process. 0.3 g Na_2S was added into 50 mL DI water and above obtained samples was added into 80 mL autoclave and kept at 120°C for 4 h.

Hybrid $NiCo_2S_4$@$NiMoO_4$ structures were fabricated by a subsequently hydrothermal method. 0.5 mM $NiCl_2$•$6H_2O$, 0.5 mM $NaMoO_4$, 0.6 g Urea and 0.3 g NH_4F were dissolved in 40 ml solution of deionized water and carried out at 160°C for 6 h. The average mass loads were 1.3 and 1.7 mg cm^{-2}, respectively.

Material characterization

X-ray diffraction analyzer (XRD, Shimadzu-7000) was used to analyze the constituent and crystallographic structure of the synthesized products with Cu Kα radiation (λ = 1.5406 Å) under 40 kV. The chemical bond states of the synthesized materials were analyzed by using an X-ray photoelectron spectrum (XPS, ESCALAB250). Scanning electron microscope (SEM, Gemini SEM 300-71-31) and transmission electron microscope (HRTEM, JEM-2100 PLUS) were used to characterize the morphology and structure of the synthesized samples.

2.2 Electrochemical measurements

The electrochemical properties of the synthesized products were tested by chi660e electrochemical workstation (Shanghai Chenhua). During the testing procedure, the Pt foil and Hg/HgO electrode were used for the purpose of the counter and reference electrodes, respectively. And, the $NiCo_2S_4$@$NiMoO_4$ product grown on Ni foam was used as working electrode. Cyclic voltammetry curves (CV), galvanostatic charge-discharge (GCD) and electrochemical impedance spectroscopy (EIS) measurements were measured in a 3 M KOH aqueous electrolyte.

2.3 Assembly of the asymmetric supercapacitor

All-solid-state supercapacitors were manufactured by using $NiCo_2S_4$@$NiMoO_4$ and AC as cathode and anode respectively, and using a separator (NKK separator, Nippon Kodoshi Corporation) and PVA-KOH gel as polymer electrolyte. Activated carbon (AC) electrode was fabricated by mixing activated carbon (AC), carbon black and 7 wt% polymer binders (polyvinylidene fluoride, PVDF) in a weight ratio of 7:2:1. A certain amount of N-methyl-pyrrolidone (NMP) was added to promote the formation of slurry. Then, the carbon slurry is coated with conductive Ni foam using a doctor blade. Finally, the prepared electrodes were dried in vacuum at 60°C for 12 h to remove all solvents.

Results And Discussion

Firstly, crystalline structure and phase purity of the products are analyzed by XRD. Figure 1a shows the XRD spectra of the samples as-prepared samples. The three samples have sharp diffraction peaks at 2 theta value of 44.5°, 51.8° and 76.4°, corresponding to the surface index (111), (200) and (220) of Ni foam the standard comparison card (JCPDS No. 04-0850), respectively. It is found that there are several distinct diffraction peaks at 21.8°, 31.1°, 37.8°, 50.1° and 55.2° corresponding to (101), (110), (003), (211) and (122) crystal planes of $NiCo_2S_4$ (JCPDS No.20–0782), respectively. Other peaks at 21.8°, 31.1°, 37.8°, 50.1° and 55.2° corresponding to (101), (110), (003), (211) and (122) crystal planes of can be indexed to $NiMoO_4$ (JCPDS No.12–0348). There is no diffraction peak of other impurities, which indicates that the sample is $NiCo_2S_4$@$NiMoO_4$ phase with high purity.

The composition and surface valence of the elements were analyzed by XPS $NiCo_2S_4$@$NiMoO_4$ samples. As shown in Fig. 2(a-d). Figure 2a shows Co 2p spectra, two distinct characteristic peaks at the binding energy of 777.8 eV and 795.1 eV, which are consistent with Co $2p_{3/2}$ and Co $2p_{1/2}$, respectively [20]. The existence of Co^{2+} and Co^{3+} can be proved by spin orbit coupling. In addition, the satellite peaks at the binding energies of 784.8 eV and 879.2 eV are named Sat., which are caused by the electronic transition in the valence band [21, 22]. Mo 3d spectra are shown in Fig. 2b. $NiCo_2O_4$@$NiMoO_4$ samples exhibit two peaks at 229.9 and 232.5 eV, which correspond to Mo $3d_{5/2}$ and Mo $3d_{3/2}$. Binding energy at 235.23, 230.4 and 226.5 eV corresponds to Mo-S bond [23, 24]. Ni 2p emission spectra are fitted with two kinds of nickel species containing Ni^{2+} and Ni^{3+} (Fig. 2c). Binding energies at 853.4 eV and 856.5 eV correspond to Ni $2p_{3/2}$ and those at 874.5 and 871.6 eV for Ni $2p_{1/2}$. Those at 787 and 873 eV could be indexed to shakeup satellites (noted as Sat.,), revealing that most of Ni exists in the form of Ni^{2+} ion [25, 26]. The S 2p spectrum in Fig. 2d shows two characteristic peaks at 162.59 eV and 163.2 eV, which can be ascribed to S $2p_{1/2}$ and S $2p_{3/2}$, respectively, indicating that the S^{2+} valence exists in $NiCo_2S_4$@$NiMoO_4$. Furthermore, a satellite peak of S was checked at 168.2 eV [27], which may be owing to the high oxidation of S on the surface of $NiCo_2S_4$@$NiMoO_4$ sample during the test procedure. XPS characterization further proved that the prepared $NiCo_2S_4$@$NiMoO_4$ sample had high purity and good crystal quality [28].

SEM and TEM were used to analyze the surface morphology and structure of as-prepared products. Figure 3(a, b) shows the SEM images of the prepared products at different magnification. Ni foam surface is covered with a three-dimensional nanosheets structures (Fig. 3a). From high magnification SEM images (Fig. 2b), it is found that adjacent nanometers are linked to each other. Figure 3(c, d) show

SEM images of hybrid $NiCo_2S_4$@$NiMoO_4$ samples, it is seen that the thickness and surface roughness of the nanosheets increased significantly, which was more conducive to the exposure of active sites. From the TEM images of Fig. 3e, a layer of nanosheets uniformly coat on the surface of $NiCo_2S_4$ nanosheest, which exhibited fill consistency with the observed SEM images. The HRTEM image of Fig. 3f shows that the lattice distances of 0.28 and 0.237 nm correspond to the (110) and (003) faces of $NiCo_2S_4$ and $NiMoO_4$, respectively.

Figure 4(a-c) shows the CV curve of $NiCo_2S_4$@$NiMoO_4$, $NiCo_2S_4$ and $NiMoO_4$ electrodes at different scan rates. At different scanning rates, there are obvious oxidation and reduction peaks, which are caused by the reversible redox reaction. With the increase of scanning rate, the positions of oxidation peak and reduction peak move to positive voltage and negative voltage respectively, and the CV curve still keeps the similar shape and envelope area becomes larger, which proves that $NiCo_2S_4$@$NiMoO_4$ electrode has the characteristics of fast charge discharge and high-rate capacity. Figure 4(d-f) shows the GCD curves of $NiCo_2S_4$@$NiMoO_4$, $NiCo_2S_4$ and $NiMoO_4$ electrodes between 0 and 0.5 V at different current densities. It can be observed that these curves are symmetrical, and each curve shows a relatively flat area, which reveals the Faraday characteristics of the electrode material and high reversibility of its Faraday reaction. In addition, the capacitance of $NiCo_2S_4$@$NiMoO_4$-8 electrode is 1102.5, 843.6, 704.5, 385.4 F g^{-1} at the current densities of 1, 2, 4 and 6 A g^{-1}, respectively.

In order to explore the electrochemical performance of the synthesized products, cycle voltammetry (CV) and galvanostatic charge-discharge (GCD) curves were measured in a three-electrode-system in 3.0 M KOH solution. Figure 5a depicts the CV curves of $NiCo_2S_4$@$NiMoO_4$, $NiCo_2S_4$ and $NiMoO_4$ electrodes at 20 mV s^{-1}. It is discovered that the envelope area of the CV curve of the $NiCo_2S_4$@$NiMoO_4$ electrode is larger than that of $NiCo_2S_4$ and $NiMoO_4$ samples, indicating that the $NiCo_2S_4$@$NiMoO_4$ electrode has a large capacitance. The GCD curves of three electrode materials at 1 A g^{-1} are shown in Fig. 5b, in which $NiCo_2S_4$@$NiMoO_4$ electrode material has longer discharge time than $NiCo_2S_4$ and $NiMoO_4$ samples, indicating its high specific capacitance. The dynamic characteristics of different electrodes in the frequency range of 100 kHz to 0.01 Hz with the amplitude of 0.01 V are analyzed by electrochemical impedance spectroscopy (EIS), as shown in Fig. 3c. In the high frequency region, the intercept of the real axis corresponds to the equivalent series resistance (Rs), and the radius of the semicircle corresponds to represents the transfer resistance (Rct). In the low frequency region, the slope of the line is attributed to the Warburg resistance [29]. The lower Rs value (0.90 $\Omega \cdot cm^2$) of $NiCo_2S_4$@$NiMoO_4$ electrode indicates that it has higher conductivity. The $NiCo_2S_4$@$NiMoO_4$ electrode showed a more vertical line along the imaginary axis, indicating that the ion diffusion process was relatively fast. $NiCo_2S_4$@$NiMoO_4$ electrode has excellent electrical conductivity. In order to study the cycle stability of three electrode materials, 10000 cycles of charge discharge experiments were carried out at 3 A g^{-1} current density. As shown in Fig. 5d, the curve tends to be stable after 2000 cycles, and the specific capacitance remains at 72.7 % after 10000 cycles, indicating that $NiCo_2S_4$@$NiMoO_4$ has good cycle stability.

In order to further explore the practical application of the as-prepared samples, the asymmetric supercapacitor (ASC) was prepared with $NiCo_2S_4$@$NiMoO_4$ as positive electrode and AC as negative electrode. The CV curves of $NiCo_2S_4$@$NiMoO_4$ electrode (0-0.6 V) and activated carbon (AC) electrode (-1.0-0 V) at three electrode mode scan rate of 50 mV s^{-1} are shown in Fig. 6a. Figure 6b shows the CV curves of ASC devices under different operating voltage windows. Therefore, the stable voltage windows of the ASC device should be 0-1.6V. Figure 6c shows the CV curves of the device at different scan rates. With the increase of scan rate, its shape of the curve remains unchanged, but its area increases gradually, which indicates that the device has excellent capacitance performance. GCD curves of the assembled capacitor under different current densities are shown in Fig. 6d. The device delivers a long discharge time of 234.2 s at 1 A g^{-1}. Figure 6e shows the Ragone diagram of $NiCo_2S_4$@$NiMoO_4$//AC ASC. The as-assembled devices possess an energy density of 37.6 W h kg^{-1} at power density of 2880 W kg^{-1}, reveals that the achieved energy density of our device is distinctly than previously reported capacitive devices[30–34]. Figure 6e shows the cycle stability of the device at 10 A g^{-1}. After 10000 charge discharge cycles, the capacitance retention of the device reaches 75.0%.

Conclusion

In summary, $NiCo_2S_4$@$NiMoO_4$ electrode material has been successfully synthesized through a simple and convenient solvothermal method. The as-obtained products have large specific capacitance of 1102.5 F g^{-1} and excellent capacitive retention, due to its unique nanosheets structure. Moreover, the as-assembled device show an outstanding energy density (37.6 W h kg^{-1} at power density of 2880 W kg^{-1}), and capacitive retention after 10000 cycles. This work developed an innovative and simple synthesis method to prepare $NiCo_2S_4$@$NiMoO_4$ electrode materials, and proved the application potential of the prepared $NiCo_2S_4$@$NiMoO_4$ nanosheets structure in energy storage equipment.

Declarations

Conflicts of interests

The authors declare no competing financial interest.

Acknowledgments:

This work was supported by Liaoning Revitalization Talents Program (XLYC1907138), the Natural Science Foundation of Liaoning Province (2019-MS-239, 2020-MS-241), the Scientific Research Fund of Liaoning Provincial Education Department (JL-1901, JL-1903, JL-1916, JL-2021), the Technology Innovation Talent Fund of Shenyang (RC190360) and Liaoning BaiQianWan Talents Program, the innovation talent fund of Liaoning Province colleges (LR2019046).

References

1. Y.N. Chen, S.M. Xu, S.Z. Zhu, R.J. Jacob, G. Pastel, Y.B. Wang, Y.J. Li, J.Q. Dai, F.J. Chen, H. Xie, B.Y. Liu, Y.G. Yao, L.G. Salamanca-Riba, M.R. Zachariah, T. Li, L.B. Hu, Millisecond synthesis of CoS nanoparticles for highly efficient overall water splitting, Nano Res. 12 (2019) 2259-2267.
2. C. Liu, W. Jiang, F. Hu, X. Wu, D. F. Xue, Mesoporous $NiCo_2O_4$ nanoneedle array as supercapacitor electrode materials with excellent cyclic stabilities, Inor. Chem. Front., 2018, 5, 835-843.
3. N. Wang, H.D. Song, H.B. Ren, J.Y. Chen, M.Q. Yao, W.Y. Huang, W.C. Hu, S. Komarneni, Partly nitrogenized nickel oxide hollow spheres with multiple compositions for remarkable electrochemical performance, Chem. Eng. J. 358 (2019) 531-539.
4. M.Z. Dai, D.P. Zhao, X. Wu, Research progress on transition metal oxide-based electrode materials for asymmetric hybrid capacitors, Chin. Chem. Lett. 31 (2020) 2177-2188.
5. X. Chen, D.M. Jiang, H.Y. Li, K. Xie, Y.H. Jiang, Y.Q. Wang, Hydrogen peroxide-induced growth of hierarchical Ni_3S_2 nanorod/sheet arrays for high performance supercapacitors, J. Colloid Interface Sci. 575 (2020) 168-176.
6. P.H. Yang, W.J. Mai, Flexible solid-state electrochemical supercapacitors, Nano Energy 8 (2014) 274-290.
7. X. Wu, S.Y. Yao, Flexible electrode materials based on WO_3 nanotube bundles for high performance energy storage devices, Nano Energy 42 (2017) 143-150.
8. W.D. He, G. Zhao, P.X. Sun, P.Y. Hou, L.L. Zhu, T.L. Wang, L.G. Li, X.J. Xu, T.Y. Zhai, Construction of longan-like hybrid structures by anchoring nickel hydroxide on yolk-shell polypyrrole for asymmetric supercapacitors, Nano Energy 56 (2019) 207-215.
9. W.T. Sun, L. Xiao, X. Wu, Facile synthesis of NiO nanocubes for photocatalysts and supercapacitor electrodes, J. Alloy. Compd. 772 (2019) 465-471.
10. Y. Liu, P.F. Hu, H.Q. Liu, J.R. Song, A. Umar, X. Wu, Toward a high-performance asymmetric hybrid capacitor by electrode optimization, Inorg. Chem. Front. 6 (2019) 2824-2831.
11. B. Li, M.B. Zheng, H.G. Xue, H. Pang, High performance electrochemical capacitor materials focusing on nickel-based materials, Inorg. Chem. Front. 3 (2016) 175-202.
12. H.Q. Liu, D.P. Zhao, P.F. Hu, K.F. Chen, X. Wu, D.F. Xue, Design strategies toward achieving high performance $CoMoO_4$@$Co_{1.62}Mo_6S_8$ electrode materials, Mater. Today Phys. 13 (2020) 100197.
13. Q. Liu, X.D. Hong, X.Y. You, X. Zhang, X. Zhao, X. Chen, M.D. Ye, X.Y. Liu, Designing hetero structured metal sulfide core-shell nanoneedle films as battery-type electrodes for hybrid supercapacitors, Energy Storage Mater. 24 (2020) 541-549.
14. F.S. Chen, C. Liu, B.H. Cui, S.M. Dou, J. Xu, S.L. Liu, H. Zhang, Y.D. Deng, Y.N. Chen, W.B. Hu, Regulated synthesis of Eutectic Ni_3S_2/NiS nanorods for quasi-solid-state hybrid supercapacitors with high energy density, J. Power Sources 482 (2021) 228910.
15. J.S. Xu, Y.D. Sun, M.J. Lu, L. Wang, J. Zhang, X.Y. Liu, One-step electrodeposition fabrication of Ni_3S_2 nanosheet arrays on Ni foam as an advanced electrode for asymmetric supercapacitors, Sci. China-Mater. 62 (2019) 699-710.

16. W.H. Xie, Z.J. Xu, W.R. Zheng, W.J. Wang, C.L. Wang, C. Zhang, H.B. Sun, Fabrication of Ni_3S_2 nanoneedle-sheets electrode material with ultrahigh areal capacity of over 15 mAh $cm^{(-2)}$, Mater. Lett. 282 (2021) 128716.
17. D. P. Zhao, M. Z. Dai, Y. Zhao, H. Q. Liu, Y. Liu, X. Wu, Improving electrocatalytic activities of $FeCo_2O_4$@$FeCo_2S_4$@PPy electrodes by surface/interface regulation, Nano Energy ,2020,72,104715.
18. Z.S. Li, B.L. Li, C.N. Liao, Z.S. Liu, D.H. Li, H.Q. Wang, Q.Y. Li, One-pot construction of 3-D graphene nanosheets/Ni_3S_2 nanoparticles composite for high-performance supercapacitors, Electrochim. Acta 253 (2017) 344-356.
19. S. J. Patil, J. H. Kim, D. W. Lee, Self-assembled Ni_3S_2//$CoNi_2S_4$ nanoarrays for ultra-high-performance supercapacitor, Chem. Eng. J. 322 (2017) 498-509.
20. L. Chen, L.X. Guan, J.G. Tao, Morphology control of Ni_3S_2 multiple structures and their effect on supercapacitor performances, J. Mater. Sci. 54 (2019) 12737-12746.
21. P.b. Geng, S.S. Zheng, H. Tang, R.M. Zhu, L. Zhang, S. Cao, H.G. Xue, H. Pang Transition metal sulfides based on graphene for electrochemical energy storage, Adv. Energy Mater. 8 (2018) 1702139.
22. H.Q. Liu, D.P. Zhao, Y. Liu, Y.L. Tong, X. Wu, G.Z. Shen, NiMoCo layered double hydroxides for electrocatalyst and supercapacitor electrode, Sci. China-Mater. 64 (2021) 581-591.
23. Z. Tian, J.H. Yin, X.M. Wang, Y.Z. Wang, Construction of Ni_3S_2 wrapped by rGO on carbon cloth for flexible supercapacitor application, J. Alloy. Compd. 777 (2019) 806-811.
24. Y. Liu, D.P. Zhao, H.Q. Liu, A. Umar, X. Wu, High performance hybrid supercapacitor based on hierarchical MoS_2/Ni_3S_2 metal chalcogenide, Chin. Chem. Lett. 30 (2019) 1105-1110.
25. Z.Y. Gao, C. Chen, J.L. Chang, L.M. Chen, P.Y. Wang, D.P. Wu, F. Xu, K.Jiang, Porous Co_3S_4@Ni_3S_4 heterostructure arrays electrode with vertical electrons and ions channels for efficient hybrid supercapacitor, Chem. Eng. J. 343 (2018) 572-582.
26. M. Shen, J.L. Liu, T.C. Liu, C.M. Yang, Y.X. He, Z.L. Li, J.H. Li, D. Qian, Oxidant-assisted direct-sulfidization of nickel foam toward a self-supported hierarchical Ni_3S_2@Ni electrode for asymmetric all-solid-state supercapacitors, J. Power Sources 448 (2019) 227408.
27. C. Liu, X. Wu, B. Wang, Performance modulation of energy storage devices: a case of Ni-Co-S electrode materials, Chem. Eng. J. 392 (2020) 123651.
28. S.D. Liu, S.C. Lee, U.M. Patil, C. Ray, K.V. Sankar, K. Zhang, A. Kundu, S. Kang, J.H. Park, S.C. Jun, Controllable sulfuration engineered NiO nanosheets with enhanced capacitance for high rate supercapacitors, J. Mater. Chem. A 5 (2017) 4543-4549.
29. H.Q. Liu, M.Z. Dai, D.P. Zhao, X. Wu, B. Wang, Realizing superior electrochemical performance for asymmetric capacitors through tailoring electrode architectures, ACS Appl. Energ. Mater. 3 (2020) 7004-7010.
30. Y. Liu, P.F. Hu, H.Q. Liu, X. Wu, C.Y. Zhi, Tetragonal VO_2 hollow nanospheres as robust cathode materials for aqueous zinc ion batteries, Mater. Today Energy 17 (2020) 100431.

31. W.T. Sun, L. Xiao, X. Wu, F. Liu, Facile synthesis of NiO nanocubes for photocatalysts and supercapacitor electrodes, J. Colloid Interface Sci. 554 (2019) 705-710.
32. S.Y. Wen, Y. Liu, F.F. Zhu, R. Shao, W. Xu, Hierarchical MoS_2 nanowires/$NiCo_2O_4$ nanosheets supported on Ni foam for high-performance asymmetric supercapacitors, Appl. Surf. Sci. 428 (2018) 616-622.
33. P. Bandyopadhyay, G. Saeed, N.H. Kim, S.M. Jeong, J.H. Lee, Fabrication of hierarchical Zn-Ni-Co-S nanowire arrays and graphitic carbon nitride/graphene for solid-state asymmetric supercapacitors, Appl. Surf. Sci. 542 (2021) 148564.
34. M.Z. Iqbal, J. Khan, Optimization of cobalt-manganese binary sulfide for high performance supercapattery devices, Electrochim. Acta 368 (2021) 137529.

Figures

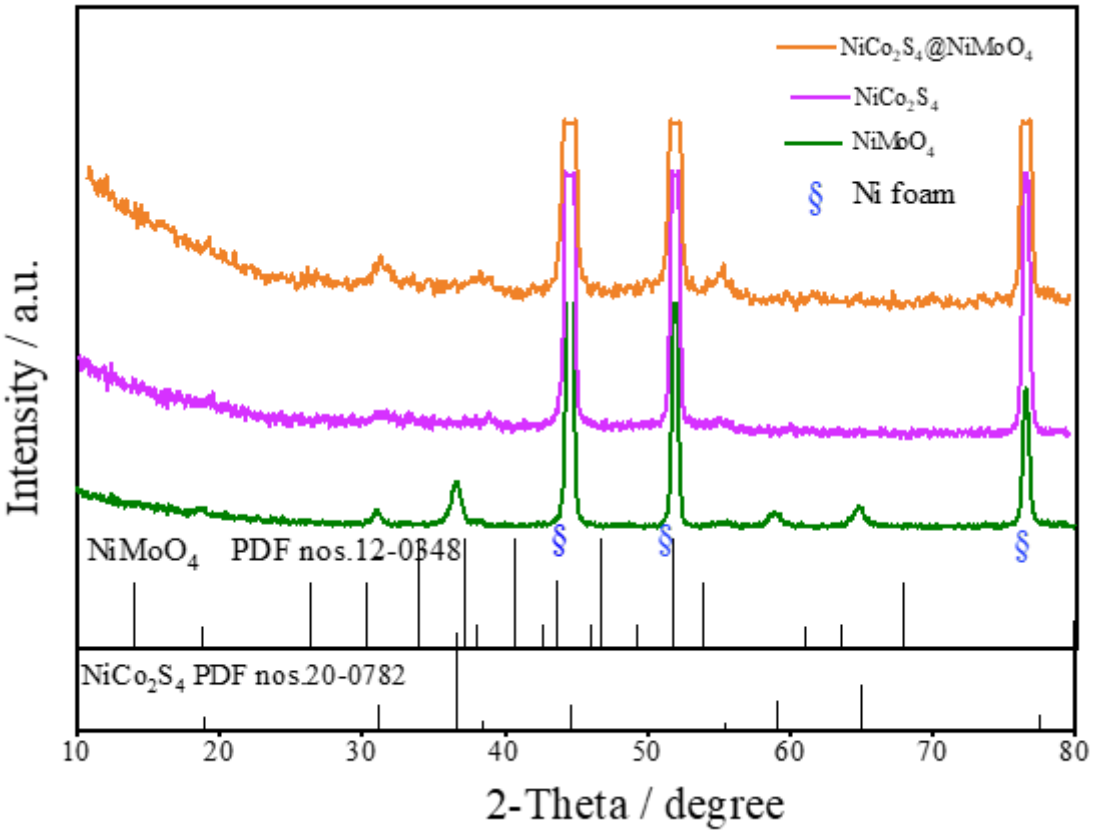

Figure 1

Structure characterization for XRD pattern of the samples

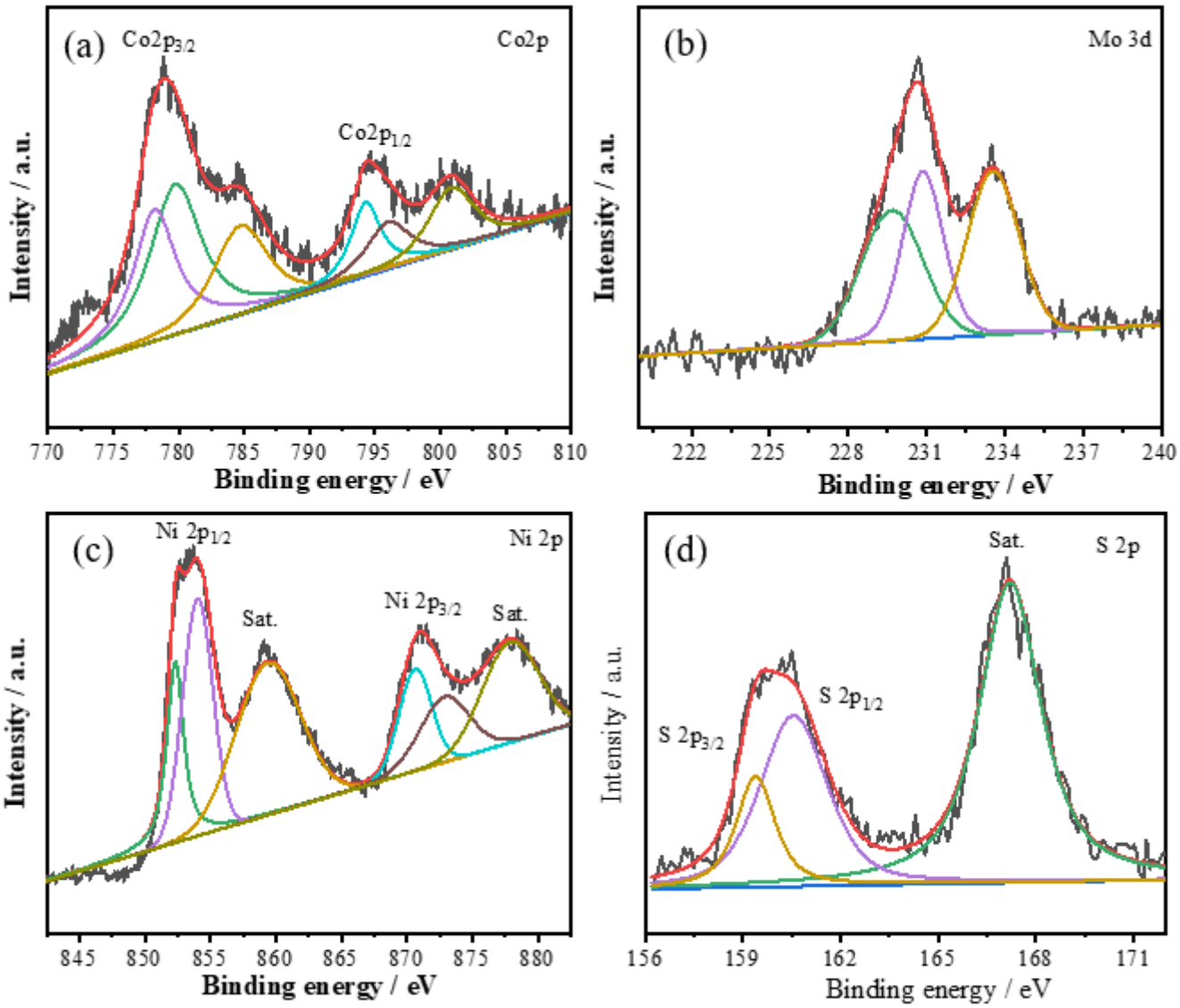

Figure 2

Structure characterization for XPS of the NiCo2S4@NiMoO4 samples (a) Co 2p (b) Mo 3d (c) Ni 2p (d) S 2p

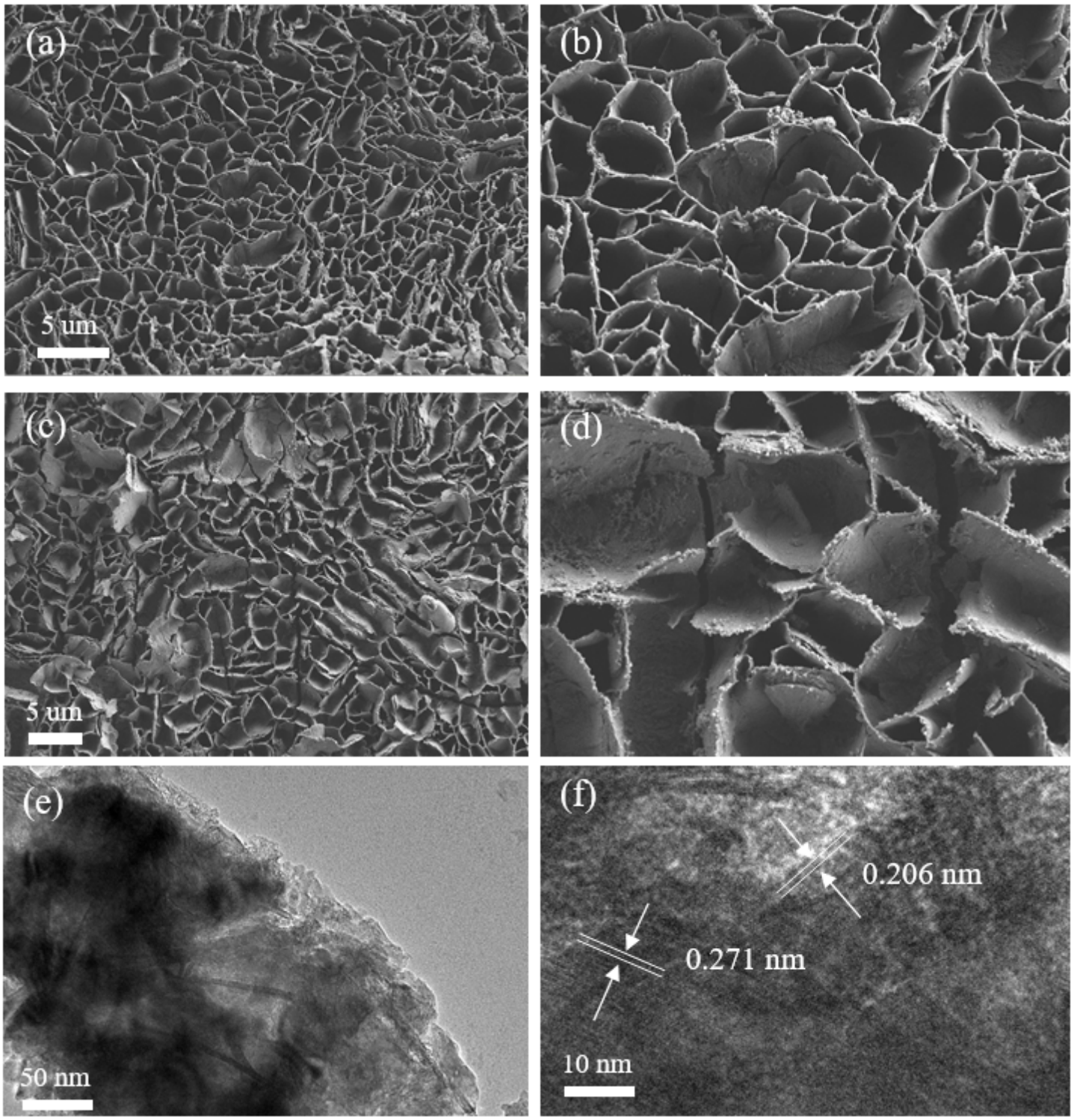

Figure 3

SEM characterization of the NiCo2S4@NiMoO4 samples (a, b) SEM images for NiCo2S4 samples (c) low magnification SEM images for NiCo2S4@NiMoO4 (d) high magnification SEM images (e, f) TEM images for NiCo2S4@NiMoO4 samples

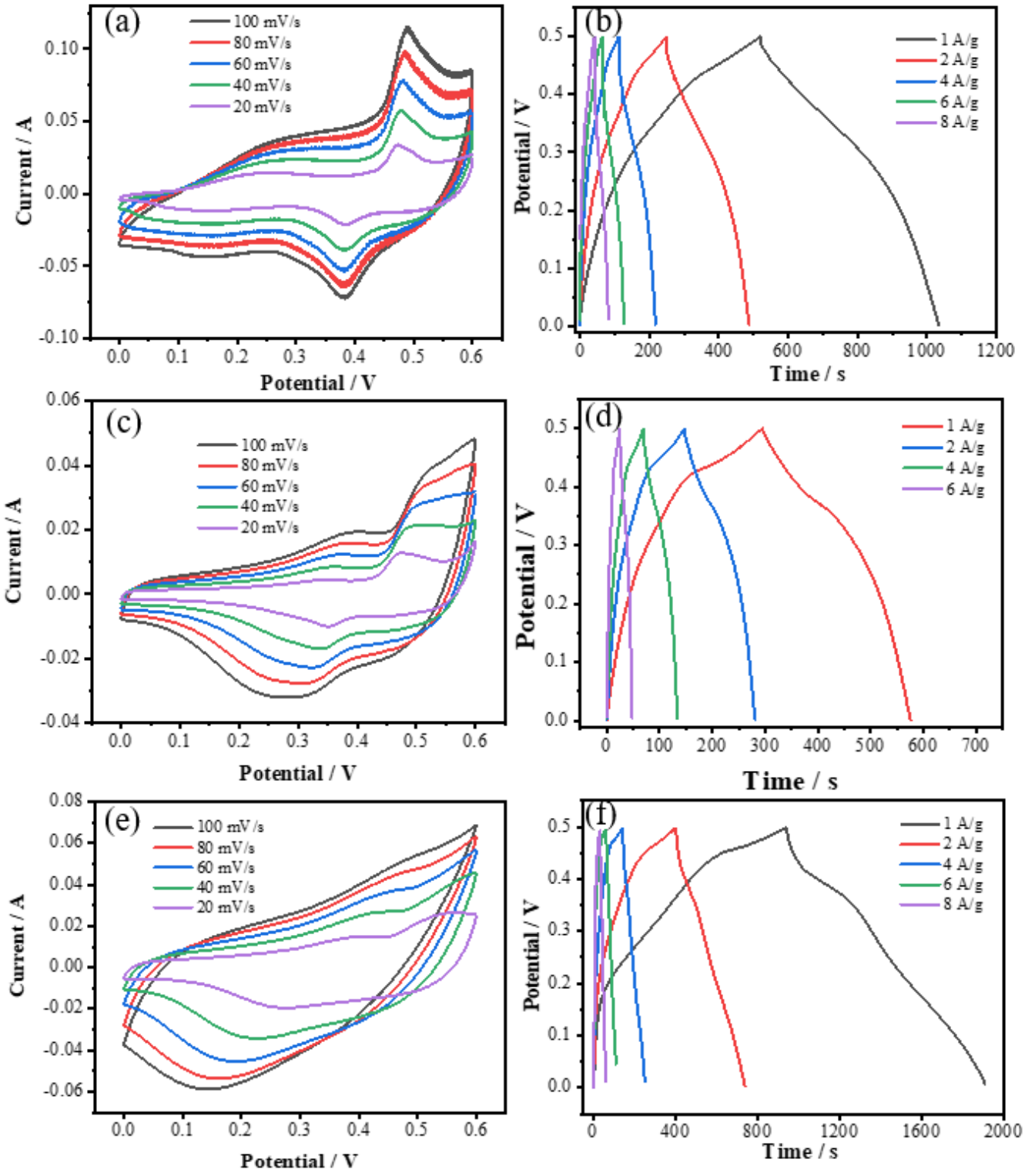

Figure 4

Electrochemical characterization of the samples (a) CV curves of NiCo2S4@NiMoO4 samples (b) GCD curves (c) CV curves of NiMoO4 samples (d) GCD curves (e) CV curves of NiCo2S4 samples (f) GCD curves

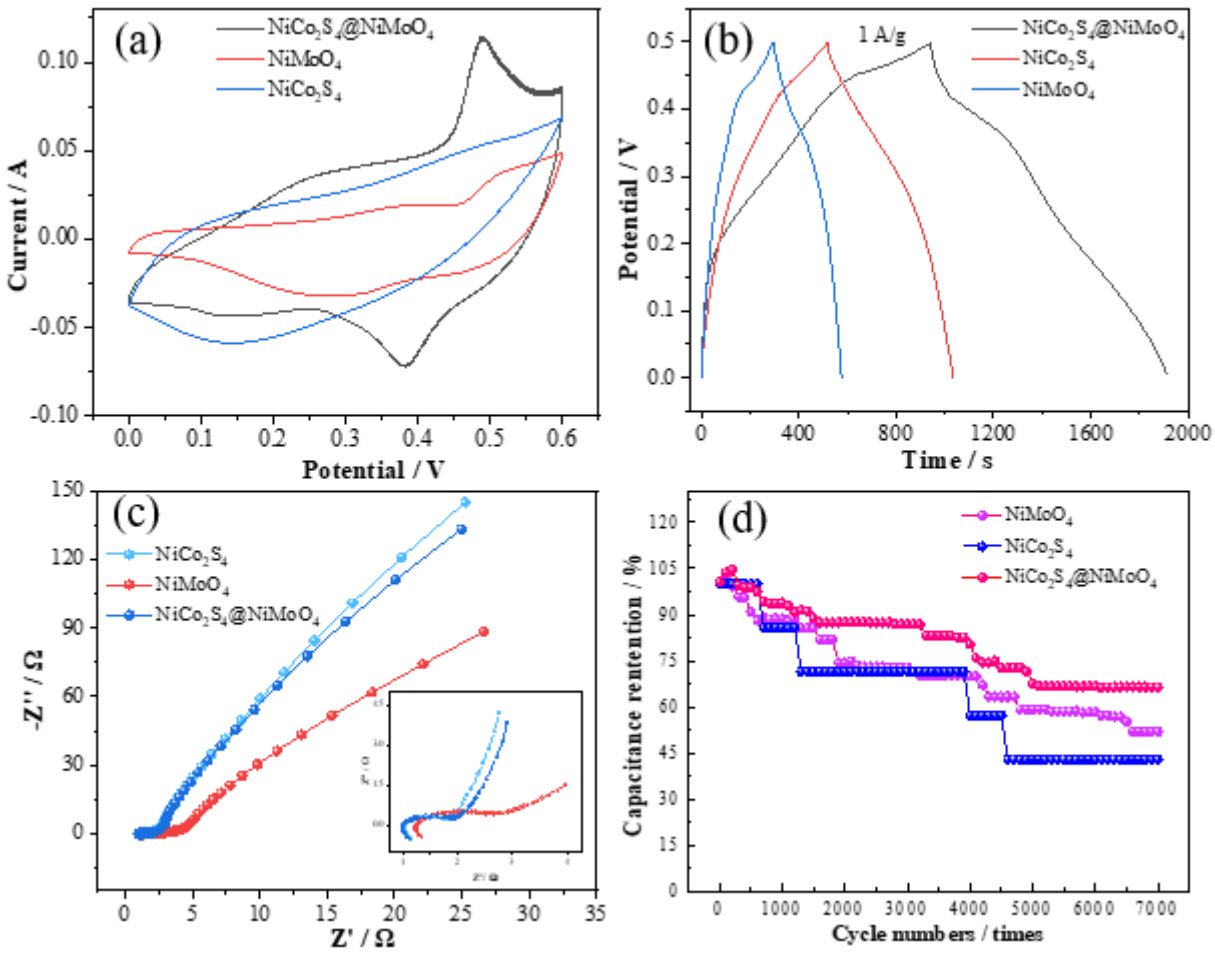

Figure 5

Electrochemical characterization of the samples (a) Comparison of CV curves of NiCo2S4@NiMoO4 samples (b) Comparison of GCD curves (c) electrochemical impedance spectroscopy (d) cycle stability

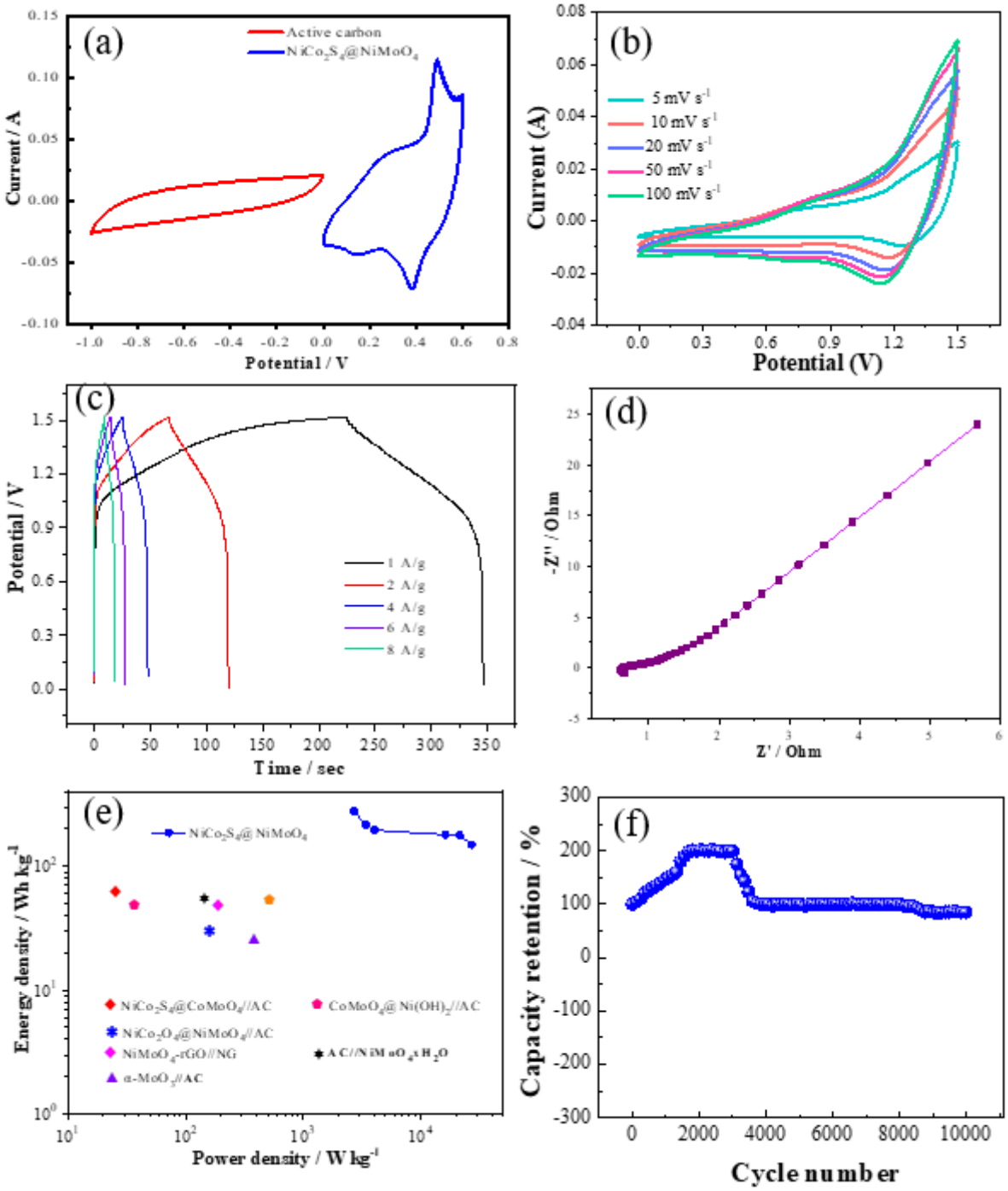

Figure 6

Electrochemical characterization of the samples (a) Comparison of CV curves of NiCo2S4@NiMoO4 samples and active carbon (b) Comparison of GCD curves (c) electrochemical impedance spectroscopy (d) cycle stability